

# Dynamics of Josephson junctions and single-flux-quantum networks with superconductor-insulator-normal metal junction shunts

A. B. Zorin, E. M. Tolkacheva, M. I. Khabipov, F.-I. Buchholz, and J. Niemeyer  
*Physikalisch-Technische Bundesanstalt, Bundesallee 100, 38116 Braunschweig, Germany*  
 (Dated: December 23, 2005)

Within the framework of the microscopic model of tunneling, we modelled the behavior of the Josephson junction shunted by the Superconductor-Insulator-Normal metal (SIN) tunnel junction. We found that the electromagnetic impedance of the SIN junction yields both the frequency-dependent damping and dynamic reactance which leads to an increase in the effective capacitance of the circuit. We calculated the dc  $I$ - $V$  curves and transient characteristics of these circuits and explained their quantitative differences to the curves obtained within the resistively shunted junction model. The correct operation of the basic single-flux-quantum circuits with such SIN-shunted junctions, i.e. the Josephson transmission line and the toggle flip-flop, have also been modelled.

PACS numbers: 74.50.+r, 84.30.-r, 73.40.Gk

## INTRODUCTION

Recently, the Josephson digital circuits operating on Single Flux Quantum (SFQ) pulses [1, 2] have been considered as electronic circuits suitable for integrating with Josephson qubits (see, for example, Refs. [3, 4]). Applying Josephson SFQ electronics for the control and readout of the qubits has many advantages, including a high speed of operation and low operating temperature in combination with rather small dissipating power, allowing a sufficiently close location of the elements on the chip. Moreover, this Rapid SFQ (RSFQ) electronics makes it possible to process the input and output signals of the qubits directly on chip. This possibility can extend the class of algorithms to be realized in the Josephson quantum computer. Finally, a similar Josephson junction fabrication technology for both, the RSFQ circuits and the qubits, is an essential prerequisite to reach a joint circuit architecture.

The operating principle of the RSFQ circuits is based on the single  $2\pi$ -leaps of the Josephson phase  $\varphi$  in the overdamped junctions. Due to large damping, the driven Josephson junctions never switch completely into the phase-running regime with a large average voltage across the junction, but generate short SFQ pulses,  $V(t) = (\Phi_0/2\pi)d\varphi/dt$ , with quantized area,  $\int V(t)dt = \Phi_0$ , where  $\Phi_0 = h/2e \approx 2.07 \times 10^{-15}$  Wb is the flux quantum [1]. For the most manufacturable Superconductor-Insulator-Superconductor (SIS) tunnel junctions with a not very large critical current density  $j_c$ , operating at a temperature which is notably below the critical temperature of the superconductor, ( $T \lesssim 0.5 T_c$ ), intrinsic damping is very small. Sufficient damping is therefore achieved due to an external low-ohmic resistance  $R_s$  shunting the junction, so the McCumber-Stewart parameter [5, 6],

$$\beta_c = \omega_c^2 / \omega_p^2 = (2\pi/\Phi_0)I_c R_s^2 C, \quad (1)$$

where  $I_c$  is the critical current and  $C$  is the junction capacitance, is small, i.e.  $\beta_c \lesssim 2$ . At such values,

the plasma resonance frequency of the Josephson junction,  $\omega_p = (2\pi I_c / \Phi_0 C)^{1/2}$ , is just slightly lower than the Josephson characteristic frequency  $\omega_c = (2\pi/\Phi_0)I_c R_s$  and the plasma oscillations are strongly damped.

Contrary to this, the operation of Josephson qubits requires vanishing damping in both the qubit's junctions and in the environment, including the coupled control and readout circuits. The effect of unsuppressed damping is, however, dramatic and appears in fast decoherence of the qubit. Especially, the noise resulting from damping at frequencies around the characteristic frequency of the qubit,  $\Omega = (E_0 - E_1)/\hbar$  (typically, about 10 GHz), causes intensive relaxation, while the low-frequency components of the noise lead to a dephasing of the qubit (see, e.g. the review [7]). At short decoherence times, qubit manipulation is unfeasible. This situation can to a certain degree be softened by weakening and/or switching on and off the coupling [8] and by operating the qubit in the optimal points where the qubit is immune to the external noise in the linear order [9, 10]. In the case of the RSFQ circuit interface coupled to the qubit, the low resistance of the junction shunts  $R$  is the source of large broad-band current noise ( $\propto R^{-1}$ ) acting on the qubit. Moreover, this noise is generated by the resistors even in the quiescent (zero-voltage) state of the Josephson junctions. So, the problem of reducing the noise of RSFQ circuits coupled to the qubit has to be solved radically.

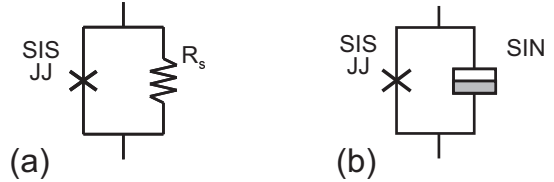


FIG. 1: Electrical circuit diagram of (a) an resistively shunted and (b) SIN-shunted SIS Josephson junction (JJ).

A promising approach based on the possibility of frequency-dependent damping of SIS junctions by means of their shunting with Superconductor-Insulator-Normal metal (SIN) tunnel elements (see Fig. 1) has recently been proposed in Ref. [11]. In particular, it was shown that shunting by a non-linear resistance drastically improves the noise characteristics of the circuit and ensure sufficient damping to achieve an almost non-hysteretic shape of the  $I$ - $V$  curves. The applied model was, however, rather simplified and the special aspects of dynamical processes not investigated. In this paper, we address the problem of a microscopic model describing the SIS+SIN circuit, as well as the analysis of the dynamics of the basic RSFQ networks within the scope of this model. The aim of this work was to demonstrate the full functionality and applicability of these circuits for the Josephson qubits.

### SIMPLE MODEL

Due to the very large values of the zero-bias differential resistance and the strongly nonlinear dc  $I$ - $V$  characteristic of the SIN junctions at low temperature ( $T \ll T_c$ ), their noise is small in the range of frequency up to  $\omega_g \equiv \Delta/\hbar$ , where  $\Delta$  is the energy gap of the superconducting electrode of the SIN junction. If the qubit's characteristic frequency is sufficiently small,  $\Omega < \omega_g$ , the influence of this noise on the qubit is expected to be weak. On the other hand, if  $\omega_g$  is lower than the characteristic Josephson frequency  $\omega_c = (2\pi/\Phi_0)I_c R$ , where  $R$  is the asymptotic resistance of the SIN junction at large bias ( $V \gg V_g \equiv \Delta/e$ ), a large effective damping of the Josephson junction is still possible at sufficiently small values of parameter  $\beta_c$  given by Eq. (1) with replacement  $R_s \rightarrow R$  [11]. The capacitance  $C$  in this equation is equal to the sum of the capacitances of the SIS and SIN elements,  $C_{\text{SIS}} + C_{\text{SIN}}$ .

For an analysis of the  $I$ - $V$  characteristics of the SIN-shunted Josephson junctions the simplified equation of motion with nonlinear conductance term was numerically solved in Ref. [11], viz.,

$$C \frac{dV}{dt} + I_{\text{SIN}}^{\text{dc}}(V) + I_c \sin \varphi = I, \quad (2)$$

where the instant voltage

$$V(t) = \frac{\Phi_0}{2\pi} \frac{d\varphi}{dt}. \quad (3)$$

Here,  $I_{\text{SIN}}^{\text{dc}}(V)$  is the dc  $I$ - $V$  characteristic of the SIN junction with the instant voltage  $V(t)$  as an argument. Equation (2) is a modified Resistively Shunted Junction (RSJ) model equation [5, 6], relating the terms taken at a given instant. Earlier, a similar model was applied for describing the quasiparticle damping in SIS junctions

by Prober et al. [12], who approximated the nonlinear conductance term by three straight line segments.

Equation (2) is, however, too rough and does not describe correctly the processes as the decay of plasma oscillations caused by a short kick of the phase in the zero-current-biased circuit. In fact, after fast exponential decay and approaching the sufficiently low level ( $\approx V_g$ ), the amplitude  $V_A$  of the oscillations  $V(t) = V_A(t) \cos \omega_p t$  starts to decrease much slower, because of small damping being available for the small instant values of voltage  $V$  according to Eq. (2). On the other hand, at sufficiently small  $\beta_c \lesssim 1$ , these oscillations should decay very fast, independent of their amplitude. To avoid this discrepancy, a more elaborate (microscopic) model of the circuit in Fig. 1b has to be applied.

### MICROSCOPIC MODEL

We will derive the current through the SIN junction starting from the tunneling Hamiltonian of Cohen, Falicov and Phillips [13],

$$H = H_0 + H_T \equiv H_S + H_N + eV N_S + H_T. \quad (4)$$

Thereby, term  $H_S$  ( $H_N$ ) is the Hamiltonian of the superconductor (normal) electrode; term  $eV N_S$  includes the finite voltage  $V$  across the junction. The tunneling is described by the Hamiltonian

$$H_T = \sum_{k,q} T_{k,q} c_k^\dagger d_q + T_{k,q}^* c_k d_q^\dagger \quad (5)$$

and is considered to be a small perturbation. Here  $c_k$  and  $c_k^\dagger$  are, respectively, the destruction and creation operators for an electron in state  $k$  in the superconductor electrode, while  $d_q$  and  $d_q^\dagger$  are the corresponding operators for the normal electrode. The nonzero (generally, non-constant) voltage  $V$  leads to the additional ac phase factors for, say, the superconductor-electrode operators,  $c_k \rightarrow c_k e^{i\varphi(t)/2}$  and  $c_k^\dagger \rightarrow c_k^\dagger e^{-i\varphi(t)/2}$ , with  $\varphi(t) = (2\pi/\Phi_0) \int^t V(t') dt'$ .

The number operators are equal to

$$N_S = \sum_k c_k^\dagger c_k, \quad N_N = \sum_q d_q^\dagger d_q, \quad (6)$$

so the tunneling current is expressed via the expectation values of the operators  $\dot{N}_S$  and  $\dot{N}_N$ ,

$$I_{\text{SIN}} = \langle \dot{I} \rangle = e \langle \dot{N}_S \rangle = -e \langle \dot{N}_N \rangle. \quad (7)$$

Applying the perturbation theory assuming adiabatic turning on from the past of the interaction  $H_T$  we obtain the standard first-order result (see, for example, Ref. [14]),

$$I_{\text{SIN}} = -\frac{i}{\hbar} \int_{-\infty}^t e^{+0(t-t')} \langle [\dot{I}(t), H_T(t')] \rangle_0 dt', \quad (8)$$

where  $\langle \dots \rangle_0$  denotes averaging over the ensemble  $H_0$ . Introducing the retarded Green's function

$$K(t-t') = i(2e/\hbar^2)\theta(t-t')\exp[+0(t'-t)] \\ \times \sum_{k,q,k',q'} T_{k,q}T_{k',q'}^* \langle [c_k^\dagger(t)d_q(t), c_{k'}(t')d_{q'}(t')^\dagger] \rangle_0, \quad (9)$$

where  $\theta(t)$  is the Heaviside step function, we finally arrive at the convolution integral expression for the current

$$I_{\text{SIN}} = \int_{-\infty}^t K(t-t') \sin \frac{\varphi(t) - \varphi(t')}{2} dt' \quad (10)$$

with function  $K$  playing the role of a memory kernel. One can see that the tunneling current depends both on the instant value of phase  $\varphi(t)$  and on its values in the past,  $\varphi(t')$ ,  $t' \leq t$ , so Eq. (10) describes the causal physical process.

Actually, the relations similar to Eqs. (9) and (10) yield the quasiparticle component of the current in the microscopic theory of the Josephson tunneling developed by Werthamer [15] and Larkin and Ovchinnikov [16] and presented in the time domain by Harris [17]. For our case of the SIN junction, the kernel  $K(\tau)$  can be easily found from its Fourier transform giving the well-known dc  $I$ - $V$  curve of the junction. In fact, in the special case of a constant voltage bias  $V \equiv V_0$  the phase  $\varphi$  runs linearly, i.e.  $\varphi = \omega_v t + \text{const}$ , where  $\omega_v = (2\pi/\Phi_0)V_0$ , and Eq. (10) yields the dc current as a Fourier integral,

$$I_{\text{SIN}}^{\text{dc}}(V) = -I_{\text{SIN}}^{\text{dc}}(-V) = \int_0^{\infty} K(\tau) \sin(\omega_v \tau/2) d\tau. \quad (11)$$

The BCS-theory-based expression for  $I_{\text{SIN}}^{\text{dc}}$  is given by the integral over the states in the energy representation,

$$I_{\text{SIN}}^{\text{dc}}(V) = \frac{1}{eR} \int_{-\infty}^{\infty} \frac{|E|[f(E) - f(E+eV)]}{(E^2 - \Delta^2)^{1/2}} dE, \quad (12)$$

where the actual range of integration is  $|E| > \Delta$  and where  $f(E) = (1 + \exp(E/k_B T))^{-1}$  is the Fermi function (see, e.g., Ref. [18]). Applying the reverse Fourier transform to Eq. (11) we obtain

$$K(\tau) = \frac{2}{\pi} \int_0^{\infty} I_{\text{SIN}}^{\text{dc}}(\Phi_0 \omega/\pi) \sin \omega \tau d\tau, \quad \tau \geq 0. \quad (13)$$

In the case of zero temperature,  $T = 0$ , when the  $I$ - $V$  curve has the hyperbolic shape,

$$I_{\text{SIN}}^{\text{dc}}(V) = [2\theta(V) - 1]\theta(|V| - V_g)(V^2 - V_g^2)^{1/2} R^{-1}, \quad (14)$$

the integral in Eq. (13) can be computed explicitly yielding

$$K(\tau) = -(2\hbar/eR)\delta'(\tau) + K_1(\tau), \quad (15)$$

where

$$K_1(\tau) = -(\Delta/eR)\theta(\tau)J_1(\omega_g \tau)/\tau. \quad (16)$$

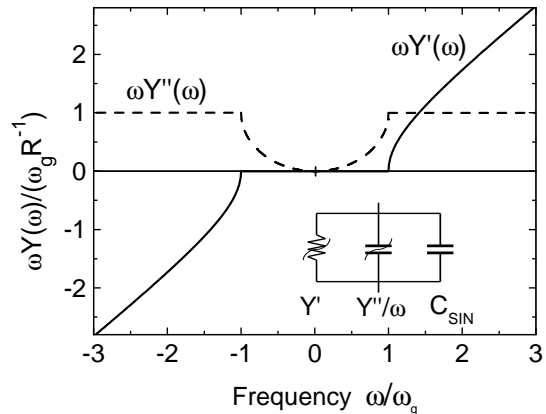


FIG. 2: Real (solid line) and imaginary (dashed line) parts of the product  $\omega Y(\omega) = \omega[Y'(\omega) + iY''(\omega)]$  calculated for the case of zero temperature,  $T = 0$ . The solid line curve also shows the shape of the dc  $I$ - $V$  curve of the SIN junction (see the first equality in Eq. (17)). The increase in temperature  $T$  leads to a rounding of the sharp corners of these curves at  $\omega = \pm\omega_g$ . The inset shows the equivalent electrical circuit of the SIN junction, which comprises (from left to right) the dynamic bias-dependent conductance, the dynamic capacitance (both frequency dependent) and the geometrical capacitance of the junction barrier.

Here  $\delta'$  is the time derivative of the Dirac delta-function and  $J_1$  is the Bessel function of the first order. The first term in Eq. (15) describes the linear component of damping due to the ohmic asymptotic at high voltage,  $|V| \gg V_g$ , while the second term, given by Eq. (16), describes the dispersive damping due to a strong non-linearity of the  $I$ - $V$  characteristic in the vicinity of  $V_g$ . (Compare the shape of the kernel Eq. (16) with  $(\pi\Delta^2/\hbar eR)\theta(\tau)J_1(\omega_g \tau)Y_1(\omega_g \tau)$ , where  $Y_1$  is the Bessel function of the second kind, obtained by Harris [17] for the SIS junction.) In the case of nonzero temperature,  $T \neq 0$ , both integrals in Eqs. (12) and (13) yielding the kernel  $K(\tau)$  should be calculated numerically.

The sine Fourier transform of the kernel  $K(\tau)$  Eq. (11) and the corresponding cosine transform give the real and imaginary parts of the junction's complex admittance, respectively,  $Y = Y' + iY''$ , viz.,

$$\omega Y'(\omega) = \frac{e}{\hbar} I_{\text{SIN}}^{\text{dc}}(\hbar\omega/2e) = \frac{e}{\hbar} \int_0^{\infty} K(\tau) \sin \omega \tau d\tau, \quad (17)$$

$$\omega Y''(\omega) = \frac{e}{\hbar} \int_0^{\infty} K(\tau) (\cos \omega \tau - 1) d\tau. \quad (18)$$

These relations arise from Eq. (10) on the assumption of a small ac voltage  $V = v_a \cos \omega t$  yielding  $\varphi = a \sin \omega t$  with  $a = 2\pi v_a/\omega\Phi_0 \ll 1$ . The corresponding real and imaginary parts of the admittance Eqs. (17) and (18) de-

terminated by the casual kernel  $K(\tau)$  obey the Kramers-Kronig relations.

As expected, the nonlinear dc  $I$ - $V$  curve  $I_{\text{SIN}}^{\text{dc}}(V)$  yields according to Eq. (17) the frequency-dependent damping  $Y'(\omega)$ . The odd function  $Y''(\omega)$  describing the junction's reactance is positive for  $\omega > 0$ , so the SIN tunnel junction behaves as an equivalent frequency-dependent dynamic capacitance  $\tilde{C}(\omega) = Y''(\omega)/\omega$  with the frequency-dependent losses  $Y'(\omega)$ , which is added up with the geometrical capacitance of the sandwich  $C_{\text{SIN}}$ . For the case of zero temperature,  $T = 0$ , the plots of the components Eqs. (17) and (18) are presented in Fig. 2, where the inset shows the equivalent electrical circuit of the SIN junction. Note that at  $\omega \rightarrow 0$ , the value of the dynamic capacitance is finite, i.e.,  $\tilde{C} = (2\omega_g R)^{-1}$ . For rather transparent barriers (for example, for the SIN junctions with an Al superconducting electrode and a specific resistance of barrier  $\rho = 30 \Omega \cdot \mu\text{m}^2$ ) this capacitance is comparable with the geometrical capacitance of the barrier (about  $50 \text{ fF}/\mu\text{m}^2$ ).

### EQUATION OF MOTION AND ITS SOLVING

For computing the SIS junction current in the circuit Fig. 1b we can naturally apply either the microscopic tunnel model [15, 16] in the form of [17] or the simpler adiabatic model of the Josephson junction giving  $I_{\text{SIS}} = I_c \sin \varphi$  [19]. In our case of significant total damping due to sufficiently low resistance  $R$  of the SIN junction [11], the quasiparticle current of the SIS junction can be neglected. Moreover, since the characteristic frequency  $\omega_c$  is appreciably lower than the gap frequency of the SIS junction  $\omega_g^{\text{SIS}} \equiv 2\Delta_{\text{SIS}}/\hbar$  ( $\Delta_{\text{SIS}}$  is the energy gap of the SIS junction electrodes, which in the most favorable case should be much larger than  $\Delta$  [20]), one can neglect the dispersion of the supercurrent. This dispersion is essential at frequencies  $\omega \approx \omega_g^{\text{SIS}}$  and manifests itself as the logarithmic Riedel peak [21]. Therefore, the model combining the microscopic description of the SIN junction and the adiabatic description of the SIS junction (with constant amplitude of supercurrent  $I_c$ ) is adequate for the circuit Fig. 1b. So, the equation of motion takes the form

$$C \left( \frac{\Phi_0}{2\pi} \right) \frac{d^2 \varphi}{dt^2} + \frac{1}{R} \left( \frac{\Phi_0}{2\pi} \right) \frac{d\varphi}{dt} + I_c \sin \varphi + \int_{-\infty}^t K_1(t-t') \sin \frac{\varphi(t) - \varphi(t')}{2} dt' = I. \quad (19)$$

Here we decomposed the kernel  $K(\tau)$  into two parts in accordance with Eq. (15), presenting the asymptotic constant contribution of damping separately, by the second term on the left-hand side.

Generally, the solving of an integro-differential equation with a slowly decaying kernel (see Eq. (16)) is a dif-

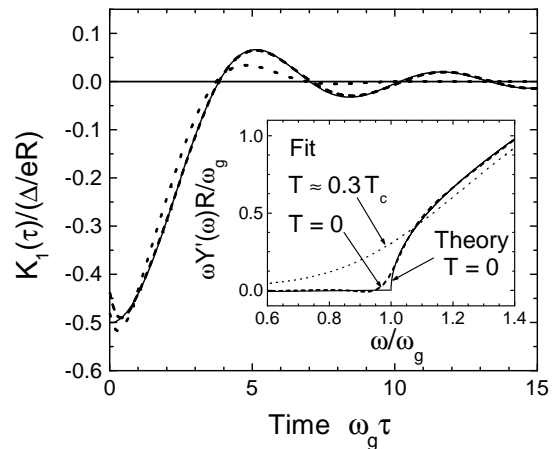


FIG. 3: Fitting of kernel  $K_1(\tau)$  Eq. (16) (solid line) by the Dirichlet series Eq. (20) with three terms (dashed line). The inessential discrepancy of the curves at small values of time  $\tau$  is related to the imperfection of the fit of the Fourier transform Eq. (17) at high frequencies,  $\omega \gg \omega_g$ . Fitting of this Fourier transform, i.e. the dc  $I$ - $V$  curve Eq. (11), in the most critical range of frequencies  $\omega \sim \omega_g$  is shown in the inset. The dotted line curves in both plots show the shape of the kernel and the  $I$ - $V$  curve given by two terms in the series Eq. (20) (coefficient  $B_2 = 0$ ) that roughly corresponds to the case of a finite temperature of  $T \approx 0.3 T_c$ .

ficult task, because at each time step  $t \rightarrow t + \Delta t$  of the numerical integration one has to take a convolution integral over the time interval from  $-\infty$  to  $(t + \Delta t)$ , that dramatically slows down such calculations. However, the calculations can be significantly accelerated if one approximates the kernel by a finite Dirichlet series [22], because the exponential shape of the kernel makes it possible to avoid the time-consuming direct integration at each step. Instead, only small corrections to the convolution integrals are computed at each time step. This procedure was realized by Odintsov et al. [23] for the kernels derived in the microscopic model of the SIS junction [15, 16]. For our case of an SIN junction having frequency dispersion of a relatively simple shape (see Fig. 2), the Dirichlet series can contain only a few terms, but still describe the dynamics adequately,

$$K_1(\tau) = \frac{\Delta}{eR} \text{Re} \sum_{n=1}^N B_n e^{p_n \tau}, \quad \tau \geq 0; \quad (20)$$

here coefficients  $B_n$  and  $p_n$  are the complex numbers with  $\text{Re}(p_n) < 0$ .

Figure 3 shows the result of the kernel fitting by the Dirichlet series Eq. (20) with  $N = 3$  for the set of frequencies:  $\text{Imp}_1 = 0.95 \omega_g$ ,  $\text{Imp}_2 = \omega_g$  and  $\text{Imp}_3 = 1.05 \omega_g$ . One can see that the approximating function captures well both the behavior of kernel  $K_1(\tau)$  and its Fourier transform (shown in the inset). Interestingly, the two-

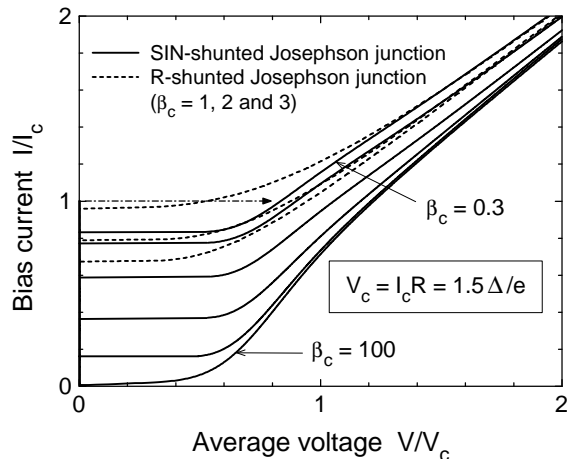


FIG. 4: The autonomous  $I$ - $V$  curves calculated within the frame of the microscopic SIS+SIN model and the RSJ model. The values of the McCumber-Stewart parameter  $\beta_c$  for the SIN-shunted junction are 0.3, 0.5, 1, 2, 5 and 100 (solid lines), while for the RSJ model the values are 1, 2 and 3 (dashed lines), in sequence from the top curve to the bottom curve. The dash-dot arrow indicates the switching from the superconducting to the resistive state due to the current bias regime. The bottom curve calculated for large  $\beta_c = 100 \gg 1$  practically coincides with the  $I$ - $V$  curve of the stand-alone SIN junction. The fragment of this curve is also shown in the inset of Fig. 3 by dotted line. The value of the characteristic voltage is equal to  $V_c = 1.5\Delta/e$  in this plot as well as in the plots which follow.

term approximation of the series Eq. (20) with the frequencies  $\text{Im}p_1 = 0.95\omega_g$  and  $\text{Im}p_3 = 1.05\omega_g$  (shown by dotted lines) yields a reasonable approximation of the dc  $I$ - $V$  characteristic for finite temperature. The obtained set of coefficients  $B_n$  and the damping factors  $\text{Re}p_n$  in Eq. (20) made it possible to reduce the numerical solving of the integro-differential equation Eq. (19) to almost that of an ordinary differential equation. For the single junction circuits the simulations were technically performed by applying the fourth-order Runge-Kutta method. For the multi-junction circuits the simulations were done with the help of the fitted program code PSCAN developed earlier for both the RSJ and the tunnel junction models [23, 24].

### JOSEPHSON JUNCTION NETWORKS WITH SIN SHUNTS

Applying the described procedure of solving the equation of motion, we first found the dc  $I$ - $V$  characteristics of the circuit Fig. 1b biased by a constant current. The resulting curves are shown in Fig. 4, where they are compared with the  $I$ - $V$  curves given by the RSJ model (Fig. 1a). One can see that the shapes of these

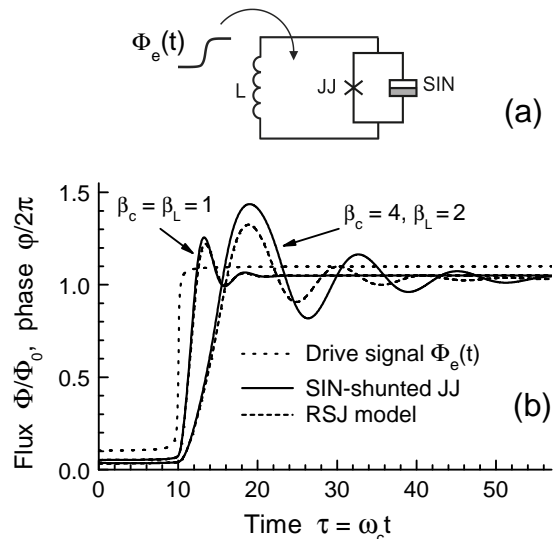


FIG. 5: (a) Electric diagram of the SIN-shunted Josephson junction inserted in the superconducting loop with the dimensionless inductance  $\beta_L = 2$  and driven by a step-pulse of the magnetic flux. (b) Switching characteristics of the SIN-shunted (solid lines) and resistively shunted (dashed lines) Josephson junctions induced by the short pulse of flux of unit amplitude  $(\Phi_e(t)/\Phi_0 = 0.1$  at  $\omega_c t < 10$  and  $1.1$  at  $\omega_c t > 10$ ) for two sets of values of  $\beta_c$  and  $\beta_L$ . The kernel  $K_1$  is approximated by two terms in Eq. (20).

curves are qualitatively similar, although the values of  $\beta_c \approx 0.3 - 0.5$  ensuring sufficiently small hysteresis in the curves for the SIN-shunted junction are appreciably smaller than the corresponding values in the RSJ model ( $\beta_c \approx 1 - 2$ ). Moreover, the former curves exhibit characteristic plateaus at  $V \lesssim \Delta/e$ . Interestingly, the size of such plateaus developed at small  $\beta_c$  is somewhat smaller than that obtained in the simplified (phenomenological) model of the SIN junction (cf. Fig. 1 of Ref. [11]).

The dynamical process of the jump of the Josephson phase by  $2\pi$  was modelled in the circuit shown in Fig. 5a. The inductance of the superconducting loop  $L$  closing the shunted SIS junction is comparable with the Josephson inductance, i.e. the dimensionless parameter

$$\beta_L = 2\pi I_c L / \Phi_0 \quad (21)$$

is equal to  $1 - 2$ . A short step-pulse of magnetic flux of the magnitude of  $\Phi_0$  was applied to the loop. The transient behavior caused by this pulse is shown in Fig. 5b. One can see that for the case of sufficiently large damping,  $\beta_c = \beta_L = 1$ , the curves for the microscopic SIN and phenomenological RSJ models practically coincide. For smaller damping, i.e. for the values  $\beta_c = 4, \beta_L = 2$  giving the bare resonance frequency of the circuit Fig. 1a equal to  $\omega_0 = \omega_c [\beta_c^{-1}(1 + \beta_L^{-1})]^{1/2} \approx 0.61\omega_c \approx 0.92\omega_g < \omega_g$ , the difference between the corresponding curves is sub-

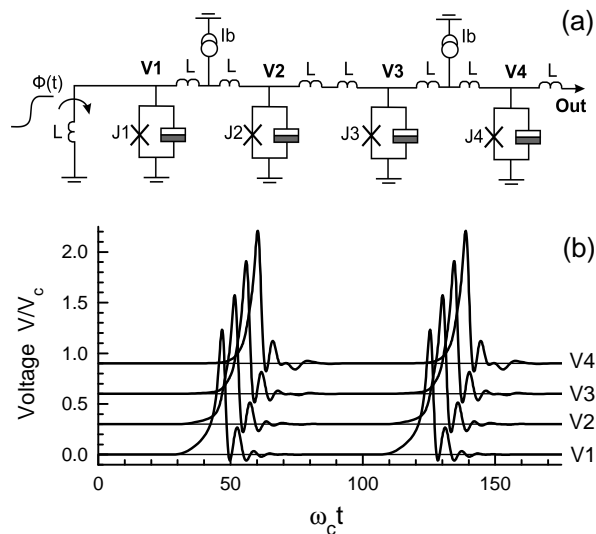


FIG. 6: (a) Electric circuit diagram of the 4-cell Josephson transmission line constructed from SIN-shunted Josephson junctions with identical critical currents  $I_c$ . The McCumber-Stewart parameter of these junctions is equal to  $\beta_c = 0.3$ . The bias currents  $I_b$  are equal to  $0.9 I_c$ . The value of each inductance is  $L = 0.4 \Phi_0 / (2\pi I_c)$ . (b) The SFQ voltage pulses on the JTL cells, corresponding to the propagation of the  $2\pi$ -leap of the phase; the voltages across different cells are offset for clarity.

stantial. The transient behavior of the SIN-shunted junction shows oscillations of larger amplitude and smaller frequency, compared to the RSJ model. The reason for this behavior is the effect of the dynamic capacitance  $\tilde{C}(\omega)$  of the SIN junction (see Fig. 2), giving  $\omega_c R \tilde{C} \approx 1.4$ . This leads to a 20% decrease in the resonance frequency  $\omega_0$ . The corresponding effective value of the McCumber-Stewart parameter  $\beta_c$  becomes therefore respectively larger.

We also present the results of simulations of the basic RSFQ circuits, i.e. the Josephson transmission line (JTL) and the toggle flip-flop (TFF) [1]. Figure 6a shows the electric circuit diagram of the JTL consisting of the chain of SIN-shunted Josephson junctions connected in parallel by relatively small superconducting inductances  $L$ . An SFQ step pulse of flux is applied to the leftmost loop of the line and causes sequential triggering of  $2\pi$ -leaps in the junctions  $J1$ ,  $J2$ ,  $J3$  and  $J4$ . As a result, the SFQ voltage pulse is transferred along the line with a small time delay,  $\sim 2\pi/\omega_c$ , on each cell (see Fig. 6b).

Figure 7a shows the electric circuit diagram of the TFF. Due to the appreciable value of the storing inductance  $L3$ , this circuit has two stable states that differ by the direction of the dc current circulating in the loop of the interferometer  $J1$ - $L3$ - $J4$ . The SFQ pulses arriving at the input port cause an alternating switching of the TFF, while the auxiliary junctions  $J2$  and  $J3$  pre-

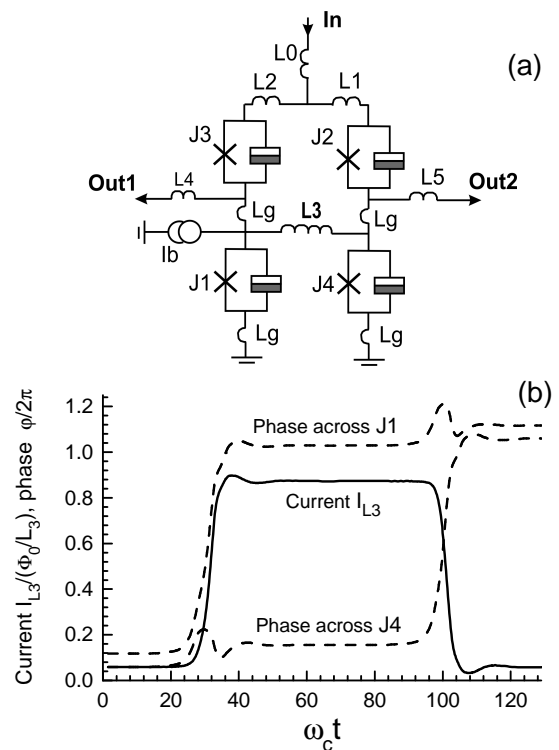


FIG. 7: (a) Electric circuit diagram of TFF constructed from the SIN-shunted Josephson junctions  $J1$ ,  $J2$ ,  $J3$  and  $J4$  having the critical currents  $I_{c1} = 1.35 I_{c0}$ ,  $I_{c2} = 1.17 I_{c0}$ ,  $I_{c3} = 1.55 I_{c0}$  and  $I_{c4} = 1.4 I_{c0}$ , respectively. The values of inductances  $L0$ ,  $L1$ ,  $L2$ ,  $L3$ ,  $L4$ ,  $L5$  and  $Lg$  expressed in units  $L_u = \Phi_0 / (2\pi I_{c0})$  are 0.4, 0.2, 0.2, 3.0, 0.8, 0.8, and 0.05, respectively. The bias current  $I_b$  is equal to  $1.31 I_{c0}$ . (b) The time dependence of the current flowing through the storing inductance  $L3$  (solid line) and the  $2\pi$ -leaps of the phases on the junctions  $J1$  and  $J4$  (dashed lines). Here the frequency  $\omega_c = (2\pi/\Phi_0) I_{c0} R$ , where the tunnel resistance  $R$  is similar for all SIN junctions.

vent a back-reaction of the interferometer on the SFQ pulse source [1]. The switching of the direction of the current circulating in the interferometer loop leads to a rectangular pulse of flux induced in inductance  $L3$  (see Fig. 7b). Such pulse, as a control signal, can, for example, be applied to the loops of the Josephson flux qubit of the double SQUID configuration [25].

## DISCUSSION

In summary, we have developed the microscopic model of the Josephson junction shunted by the nonlinear element based on the SIN tunnel junction. The behavior of the circuit is adequately described by the integro-differential equation with a memory kernel reflecting the casual dependence of the tunneling current on the phase across the junction. In contrast to the simplified model

proposed in Ref. [11], this model captures the expected features in the behavior of the SIN-shunted Josephson circuits, including a clear dependence of the decay of plasma oscillations on their frequency.

Besides the frequency-dependent damping, the SIN-junction shunts have the effect of an enhanced capacitance. The resulting capacitance includes both the geometrical capacitance of the junction and the dynamic frequency-dependent capacitance that affects the shape of the  $I$ - $V$  curve increasing the hysteresis. That is why the calculated  $I$ - $V$  curves are almost similar to those given by the RSJ model for somewhat larger values of the McCumber-Stewart parameter, i.e.  $\beta_c^{\text{RSJ}} = 1$ -3. Still, the values  $\beta_c \approx 0.3$  ensuring a sufficiently small hysteresis in SIN-shunted Josephson junctions and the functionality of the multi-junction circuits seem to be feasible. The most challenging condition to be met is the realization of high-quality SIN junctions with a high transparency of the tunnel barrier, having a specific resistance  $\rho \lesssim 30 \Omega \cdot \mu\text{m}^2$  [11]. The recent experiments with Nb-AlO<sub>x</sub>-Al (at  $T \geq 1.4$  K) and Al-AlO<sub>x</sub>-Cu (at  $T \leq 1$  K) junctions have shown that the ratio of the zero-bias resistance to the asymptotic tunnel resistance can achieve sufficiently large values, i.e.  $> 30$ – $50$  [26, 27]. (This behavior of the SIN junctions can be roughly described by the two-term approximation of the memory kernel Eq. (20).) Using such SIN junctions as shunts for Nb SIS junctions can make it possible to significantly reduce the noise of the circuits in the quiescent state in the frequency range up to  $\Delta_{\text{Al}}/h \approx 50$  GHz, i.e. within the working frequency range of the Josephson qubits of different types.

Finally, the modelled behavior of the simple RSFQ networks (JTL and TFF) is qualitatively similar to that of the conventional (resistively shunted) circuits. A preliminary evaluation of the ranges of functionality was found to be quite good. The simulation of more complex circuits can be easily performed using the slightly modified code PSCAN developed earlier for the tunnel junction model [23, 24]. So, RSFQ networks with SIN-shunts implemented in the shell that surrounds a Josephson qubit core offer a promising approach to achieve joint RSFQ-qubit operation.

## ACKNOWLEDGMENTS

We wish to thank D.V. Balashov, F. Chiarello, S. V. Lotkhov, F. Maibaum and M. Wulf for useful discussions and assistance at different stages of this work. The work was supported by the EU through the RSFQubit and SQUBIT-2 projects and DFG through the project Ni 253/7-1.

- 
- [1] K.K. Likharev and V.K. Semenov, IEEE Trans. Appl. Supercond. **1**, 3 (1991).
  - [2] P. Bunyk, K.K. Likharev and D. Zinoviev, Int. J. High Speed Electron. Syst. **11**, 257 (2001).
  - [3] V.K. Semenov and D.V. Averin, IEEE Trans. Appl. Supercond. **13**, 960 (2003).
  - [4] T.A. Ohki, M. Wulf and M.F. Bocko, IEEE Trans. Appl. Supercond. **15**, 837 (2005).
  - [5] D.E. McCumber, J. Appl. Phys. **39**, 3113 (1968).
  - [6] W.C. Stewart, Appl. Phys. Lett. **12**, 277 (1968).
  - [7] Yu. Makhlin, G. Schön and A. Shnirman, Rev. Mod. Phys. **73**, 357 (2001).
  - [8] J. Clarke, T.L. Robertson, B.L.T. Plourde, A. García-Martínez, P.A. Reichardt, D.J. van Harlingen, B. Chesca, R. Kleiner, Y. Makhlin, G. Schön, A. Shnirman and F.K. Wilhelm, Phys. Scripta **T102**, 173 (2002).
  - [9] D. Vion, A. Aassime, A. Cottet, P. Joyez, H. Pothier, C. Urbina, D. Esteve and M.H. Devoret, Science **296**, 886 (2002).
  - [10] A.B. Zorin, Zh. Éksp. i Teor. Fiz. **125**, 1423 (2004) [JETP **98**, 1250 (2004)].
  - [11] A.B. Zorin, M.I. Khabipov, D.V. Balashov, R. Dolata, F.-I. Buchholz, and J. Niemeyer, Appl. Phys. Lett. **86**, 032501 (2005).
  - [12] D.E. Prober, S.E.G. Slusky, R.W. Henry and L.D. Jackel, J. Appl. Phys. **52**, 4145 (1981).
  - [13] M.H. Cohen, L.M. Falicov and J.C. Phillips, Phys. Rev. Lett. **8**, 316 (1962).
  - [14] G. Rickayzen, *Theory of Superconductivity* (Wiley, New York, 1965).
  - [15] N.R. Werthamer, Phys. Rev. **147**, 255 (1966).
  - [16] A.I. Larkin and Yu.N. Ovchinnikov, Zh. Eksp. Teor. Fiz. **53**, 2159 (1966) [Sov. Phys.—JETP **24**, 1035 (1967)].
  - [17] R.E. Harris, Phys. Rev. B **13**, 3818 (1976).
  - [18] M. Tinkham, *Introduction to Superconductivity* (McGraw-Hill, New York, 1996).
  - [19] B.D. Josephson, Adv. Phys. **14**, 419 (1965).
  - [20] The condition  $\Delta_{\text{SIS}} \gg \Delta$  can be fulfilled, for example, for the pair of a Nb SIS junction and a SIN junction with Al superconductor electrode.
  - [21] E. Riedel, Z. Naturforsch. **19a**, 1634 (1964).
  - [22] T.M. Apostol, *General Dirichlet Series and Bohr's Equivalence Theorem* (Springer-Verlag, New York, 1997).
  - [23] A.A. Odintsov, V.K. Semenov and A.B. Zorin, IEEE Trans. Magn. **23**, 763 (1987).
  - [24] S.V. Polonsky, V.K. Semenov and P.N. Shevchenko, Supercond. Sci. Technol. **4**, 667 (1991); S.V. Polonsky, P.N. Shevchenko, A. Kirichenko, D. Zinoviev, and A. Rylyakov, IEEE Trans. Appl. Supercond. **7**, 2685 (1997).
  - [25] F. Chiarello, P. Carelli, M.G. Castellano, C. Cosmelli, M.I. Khabipov, R. Leoni, G. Torrioli, and A.B. Zorin, 10th International Superconductive Electronics Conference, September 5-9, 2005, Noordwijkerhout, The Netherlands. *Extended Abstracts*, edited by H. Rogalla and A. Brinkman (University of Twente, The Netherlands, 2005), P-C.04.
  - [26] D.V. Balashov, M.I. Khabipov, A.B. Zorin, S.A. Bogoslovsky, F.-I. Buchholz, and J. Niemeyer, 10th International Superconductive Electronics Conference, Septem-

ber 5-9, 2005, Noordwijkerhout, The Netherlands. *Extended Abstracts*, edited by H. Rogalla and A. Brinkman (University of Twente, The Netherlands, 2005), P-C.06.

[27] S. V. Lotkhov, D. V. Balashov et al., to be published.